

# Gas Flow Sputtering of Pt/C Films and their Performance in Electrocatalytic Hydrogen Evolution Reaction

Denis Bernsmeier,<sup>[a]</sup> Sören Selve,<sup>[b]</sup> Jörg Nissen,<sup>[b]</sup> Natalia Maticiuc,<sup>[c]</sup> Josefa Ibaceta-Jaña,<sup>[d]</sup> Bernd Szyszka,<sup>[d]</sup> and Ruslan Muydinov\*<sup>[c, d]</sup>

A single step deposition technique of Pt/C films for electrocatalytic applications is presented. The hollow cathode gas flow sputtering (GFS) method allows a catalyst production within few minutes without further steps. The herein presented films consist of small Pt nanocrystals (2–5 nm) deposited in a matrix of nanocrystalline carbon. The films show a low and stable overpotential under acidic conditions in the hydrogen evolution reaction (HER). Relatively low Pt-mass activity ( $< 1 \text{ mA}/\mu\text{g}_{\text{Pt}}$ ) is attributed to the yet too high Pt-content in the films. Another

issue discovered in this work is a non-graphitic state of carbon resulting in its high resistivity. Still, the GFS deposition technique providing by nature high deposition rates and a substance-to-material yield of 80–90% is advantageous than other sputtering techniques and especially chemical methods in that sense. This technique is scalable to areas in the range of square meters and thus represents an attractive way to efficiently produce large-scale cathode coatings for industrial electrolyzers.

## Introduction

The use of hydrogen as an energy carrier becomes more and more important. Catalysts play a key role for an efficient hydrogen production via electrolysis. Especially under acidic conditions, at the cathode of PEM electrolyzers Pt-based catalysts still show the highest performance in terms of activity and stability in the hydrogen evolution reaction (HER).<sup>[1]</sup> Being actively developed, noble metal free materials become better and more attractive.<sup>[2–5]</sup> Yet, Pt nanoparticles on conductive carbon still are the most commonly employed catalytic system.<sup>[6–8]</sup> Chemical nature, size and distribution of metal particles, as well as allotropic form and surface area of the carbon carrier influence their catalytic activity. Apart from the wide use of platinum in the electrocatalytic HER,<sup>[9,10]</sup> platinum also catalyses other reactions: e.g. oxidation of ammonia,<sup>[11]</sup> glycerol,<sup>[12]</sup> aromatic compounds,<sup>[13]</sup> dehydrogenation of

tetralin,<sup>[14]</sup> and decalin<sup>[15]</sup> as well as hydrogenation of aromatic compounds,<sup>[16]</sup> and fatty acids.<sup>[17]</sup> Pt/C composites may also store gaseous hydrogen.<sup>[9]</sup>

Pt/C catalysts are typically prepared by the impregnation of a carbon support with a Pt-containing solution.<sup>[9,10,12,14,15,18]</sup> When solutions of Pt ions are employed, this technique requires a following reductive treatment to yield metallic Pt particles. Usual carbon supports are powders of carbon nanotubes,<sup>[12,14,15,18]</sup> activated carbon<sup>[9]</sup> or carbon black.<sup>[10]</sup>

Electrocatalysis requires homogeneous and stable coatings. One approach is an ink-based casting which often leads to inhomogeneities of the coating.<sup>[19,20]</sup> Moreover, the use of binding agents, like Nafion, may block pores and catalytically active sites.<sup>[21–33]</sup> Another approach are Pt-containing carbon coatings with controlled porosity and high electrical conductivity, so called ordered mesoporous carbon (Pt/OMC) coatings.<sup>[25]</sup> Such materials show an enhanced thermal and electrochemical stability but have small Pt weight-loadings. A heat treatment removing the template polymer and converting precursor into a carbon matrix are required.

In summary, wet chemical methods have several technological issues: they are multistage, deal with complex chemistry and can include high temperature treatments.

In that sense, sputtering looks promising as an established deposition method already used on industrial scale for numerous materials. It also allows depositing nanostructured catalysts in general,<sup>[34,35]</sup> and Pt/C in particular.<sup>[36,37]</sup> Sputtered Pt/C catalysts were successfully tested in fuel cells,<sup>[36–39]</sup> sensors,<sup>[40]</sup> and as catalyst for methanol oxidation.<sup>[41]</sup> Sputtered catalysts with low Pt-loadings show a strong catalytic performance in Proton Exchange Membrane Fuel Cells (PEMFCs).<sup>[38,42]</sup>

The hollow cathode gas flow sputtering (GFS) is advantageous in comparison to the magnetron sputtering since it works at higher process pressure (mbar range) and provides relative compositional freedom. GFS plasma is characterized by a high ionization degree, a high electron flux and a low

[a] Dr. D. Bernsmeier  
Department of Chemistry  
Technical University Berlin  
Straße des 17. Juni 124, 10623 Berlin (Germany)

[b] S. Selve, J. Nissen  
Zentraleinrichtung Elektronenmikroskopie (ZELMI)  
Straße des 17. Juni 135, 10623 Berlin (Germany)

[c] Dr. N. Maticiuc, Dr. R. Muydinov  
PVcomB,  
Helmholtz-Zentrum Berlin für Materialien und Energie GmbH  
Schwarzschildestraße 3, 12489 Berlin (Germany)  
E-mail: ruslan.muydinov@campus.tu-berlin.de

[d] J. Ibaceta-Jaña, Prof. B. Szyszka, Dr. R. Muydinov  
Chair Technology for Thin Film Devices  
Institute of High-Frequency and Semiconductor-system Technologies  
Technical University Berlin,  
Einsteinufer 25, 10587 Berlin (Germany)

Supporting information for this article is available on the WWW under <https://doi.org/10.1002/cphc.202200650>

© 2023 The Authors. ChemPhysChem published by Wiley-VCH GmbH. This is an open access article under the terms of the Creative Commons Attribution License, which permits use, distribution and reproduction in any medium, provided the original work is properly cited.

temperature of neutrals and ions.<sup>[43–45]</sup> In this work, we evaluate the applicability of the GFS method to produce nanostructured Pt/C catalyst films in a single-step process.

## Experimental Section

The Pt/C films were obtained in one deposition step using a GFS system schematically shown in Figure 1 and described elsewhere.<sup>[46]</sup> The tubular Pt/C target with an inner diameter of 40 mm and 5 mm thick walls consisted of two ~30 mm graphite segments (99.99%, Kornmeyer Graphit GmbH) and one 1 mm thick Pt (99.99%, Avaluxe) ring in the middle. The latter was the lowest commercially available thickness.

Power generation was realised by a 10 kW TruPlasma DC 4100 (TRUMPF Hüttinger) device having besides a direct current (DC) mode also an unipolar pulsing mode working in a middle frequency (MF) range. The maximal possible frequency and reverse voltage are 100 kHz and +100 V, respectively. These parameters were applied to remove the negative charging of the substrate surface. Argon (99.999%) was used as sputtering gas. The basic pressure was ~1 Pa and the process pressure was held at 34 Pa. In a blank (plasma free) experiment,  $p(\text{O}_2)$  was measured above the substrate using a vacuum oxygen sensor (model XS22.112H-450 from ZIROX Sensoren und Elektronik GmbH). A power of 500 W and a target-to-substrate distance of 1.5 cm were chosen based on preliminary experiments. At a static deposition, the homogeneous area has a circular shape with a diameter of > 30 mm. Using a Pt-free graphite target and varying power (500 W vs. 1000 W) at a substrate-to-target distance of 1.5 cm and 3.5 cm, respectively, we obtained carbon films with densities in the range 1.3...2 g/cm<sup>3</sup> as estimated using XRR. These values vary within the range 60...90% of theoretical graphite density.

To exclude analytical signal from the substrate, 1.1 mm thick Corning Eagle XS glass was used to produce Pt/C-samples for X-ray diffraction (XRD) / X-ray reflectometry (XRR) and conductivity measurements. For transmission electron microscopy (TEM), scanning electron microscopy (SEM), electron micro-probe analysis (EPMA), Raman and X-ray photoelectron spectroscopy (XPS) measurements, 0.45 mm thick silicon wafers were used as substrates to provide conductivity. Pt/C films for catalytic measurements were deposited on 1 mm thick Glassy Carbon plates (HTW Hochtemperatur-Werkstoffe GmbH). All substrates were sonicated prior to the deposition in organic solvents and de-ionised water at 45 °C. All three kinds of substrate were deposited at once in each deposition

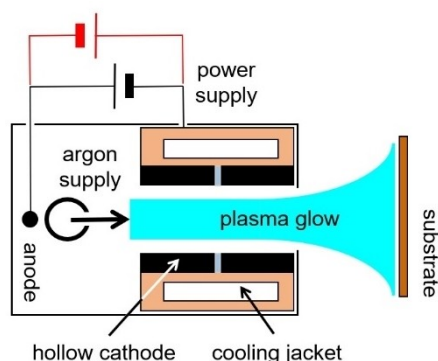


**Figure 1.** Principle scheme of the GFS deposition shown in cross-section. Tubular hollow target had two ~30 mm long graphite segments (shown in black) and in the middle – 1 mm thick platinum ring (in grey).

case. During deposition no intentional heating of a substrate was applied.

The film thickness was evaluated by a Dektak 6 M (Bruker) profilometer with a stylus of 2.5 μm radius and 3 mg of applied weight. Based thickness vs. deposition time dependence the deposition rate was determined.

For the TEM investigation, the specimen slice was prepared by Focused Ion Beam (FIB) using a FEI / Thermofisher Helios Nanolab 600. To protect the specimen from the damage during a Ga<sup>+</sup> milling process, tungsten cap layers of ~50 nm and ~700 nm thickness were grown respectively by electron beam-induced deposition (EBID) and ion beam-induced deposition (IBID). The thinning was performed at 30 kV starting with a current of 460 pA and reducing it to 28 pA. Finally, the lamella was exposed to Ga<sup>+</sup> ions accelerated at 2 kV to reduce the amorphous layer on the surface. The ready sample was transferred to a Cu Omniprobe grid and stored under vacuum. TEM, high resolution TEM (HRTEM) and electron diffraction investigations were performed at a FEI TECNAI G<sup>2</sup>20 S-Twin transmission electron microscope with a LaB<sub>6</sub> emitter, operated at 200 kV. TEM images were acquired with a Gatan 1k×1k MSP794 P CCD-camera. For further TEM investigations the specimen was oriented along a <110> zone axis of Si, to measure perpendicular to its <100> direction. The thickness of the FIB lamella was extrapolated from the Si-substrate via comparative convergent beam electron diffraction (CBED) measurements and simulations.

SEM images were acquired on a JEOL 7401F system at 10 kV acceleration voltage.

The geometric Pt- and C-loading was studied by field emission electron-probe microanalysis (FE-EPMA) using the JEOL JXA-8530F (Japan) device. For the quantitative analysis an acceleration voltage of 5 kV and a probe current of 31 nA were used. The probe diameter and the measurement time were 18 μm and 20 s respectively. Five points were probed in each sample. As references, metallic platinum standard (99.95%), carbon standard (99.99%) and silicon standard (99.9995%) were used for the determination of corresponding elements. Pt and Si were analysed with a PETH-crystal and C with a LDE2-crystal. The data were evaluated with the Strata-Gem Software.

Two-point electrical conductivity measurements were conducted using a Keithley Source Measurement Unit, Model 6517B, employing an 8×8 pin (6.5×6.5 mm<sup>2</sup> area) probe head. Geometrical factors of the probe head were taken into account by measuring a standard indium-tin oxide (ITO) film sample.

The grazing incidence (GI) XRD measurements were performed at  $\omega = 1^\circ$  on D8 Discover (Bruker AXS, Germany) instrument with Cu K<sub>α</sub> irradiation, Göbel-mirror and secondary equatorial soller (2.5°). Detector scanning was conducted with a step size of 0.03° and 20 s acquisition time. At these conditions the entire depth of the film was probed. Instrumental broadening was determined using a polycrystalline Al<sub>2</sub>O<sub>3</sub> standard from Bruker AXS. The XRR measurements were performed using a Göbel-mirror and the following set of slits: 0.2 mm primarily and 0.6 mm→0.2 mm secondarily. A coupled scan had 0.01° and 2 s acquisition steps.

Micro-Raman spectroscopy was performed in a high-resolution Horiba LabRAM HR800 spectrometer. The excitation wavelength and applied power intensity were 532 nm and 21.3 mW, respectively. Spectra were acquired using a 100-fold magnification lens, 400 μm hole aperture, grating with 600 lines per mm and 30 s acquisition time.

The XPS measurements were performed in a standard XPS laboratory module with a non-monochromatic Al K<sub>α</sub> X-Ray source.

After a very short air exposure, the samples were mounted onto the holder in a dried N<sub>2</sub>-filled glovebox. XPS spectra were collected at 100 eV and 20 eV passing energy for survey and detailed regions, respectively, and were calibrated to C1s peak corresponding to the adventitious carbon (285 eV).

Electrochemical testing was performed in a three-electrode setup with a rotating disk working electrode.<sup>[47]</sup> Disks of the exposed diameter 5 mm were cut out from the catalyst coated glassy carbon plates by a laser (FiberScan SQ, Siro Lasertec). Pt mesh was used as the counter electrode and a reversible hydrogen electrode (Gaskatel, HydroFlex) served as the reference electrode. The electrolyte, 0.5 mol/l H<sub>2</sub>SO<sub>4</sub> (Fixanal, Fluka Analytical) solution, was purged with nitrogen gas prior to the electrocatalytic test. The measurement protocol was as follows: (i) 50 cyclic voltammograms at a scan rate of 20 mV/s in the HER regime, (ii) chronopotentiometry in the HER regime, (iii) 1000 cyclic voltammograms between 0.05 V and 1.2 V with the scanning rate 100 mV/s. Between each block the potentiostatic impedance spectroscopy at 500 mV was performed for iR correction.

## Results and Discussion

The type of power generation – direct current DC or unipolar pulsing in middle frequency MF – has only a slight influence on the film characteristics. A comparison between DC and MF pulsed sputtering regimes is given in Supporting Information (SI, Table S1 and Figure S1). The Pt-content in the composite Pt/C-films was found to be much higher than one could expect from the geometrical constitution of the target. This circumstance results from an about one order of magnitude higher sputtering rate of platinum as compared to the same of carbon.<sup>[48]</sup> The Pt-load is generally higher in MF-films than in DC-films. At the same time, deposition rate at 500 W differs as follows: 40 nm/min for the DC- and 60 nm/min for the MF-mode. An average density value estimated from the XRR curves are respectively 11.4 and 8.2 g/cm<sup>3</sup> (Figure S1). These values being clearly between densities of graphite (2.25 g/cm<sup>3</sup>) and metallic platinum (21.45 g/cm<sup>3</sup>) show that the DC-film is denser than the MF-one. A nanostructure appears to be similar for the corresponding films. The cross-section TEM images reveal 2–5 nm small Pt-nanoparticles in a carbon matrix (Figure 2) and a continuous morphology throughout the film volume (Figure S2). One may speculate, that Pt-nanoparticles are smaller and more separated in the MF-film. The film slices had however thickness of few tens of nanometres that may result in overestimation of diameter and density of Pt-nanoparticles. The electron diffraction maxima (Figure S2) correspond solely to the cubic platinum phase with lattice constant  $a = 3.92 \pm 0.03 \text{ \AA}$  for the DC film and  $3.93 \pm 0.03 \text{ \AA}$  for the MF film.

The surface microstructures from in-plane view SEM of both films looks similarly homogeneous and free of open pores (Figure 2c,d). Beyond that the MF-film looks somewhat rougher.

The GI-XRD patterns of corresponding films deposited on glass are shown in Figure 3. All broad reflections can be assigned to a fcc-Pt phase. The Scherrer equation gives an estimated size of defect-free crystalline areas of ~1.5 nm for the DC- and ~1.7 nm for the MF-film. In this respect one may speculate that the crystallites as they appear in TEM contain

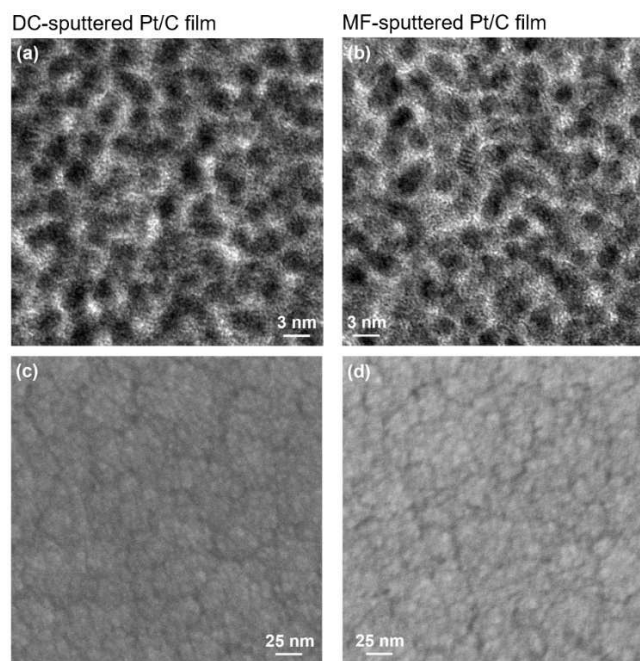


**Figure 2.** Cross-sectional TEM images and plane-view SEM images for the DC- (a,c) and MF-sputtered (b,d) Pt/C films.

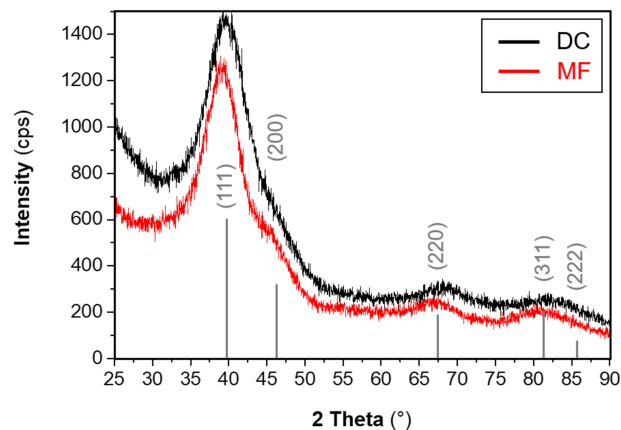


**Figure 3.** GI-XRD patterns of the ~240 nm thick Pt/C films on glass. Two deposition regimes are compared. The bars correspond to the cubic Pt phase standard (PDF 00-004-0802).

many defects. An estimation of the lattice constants from these XRD patterns is inaccurate, yet the relative peak positions correspond to a smaller lattice constant in the DC film that agrees with results of electron diffraction. It is known that fcc-Pt lattice expands at initial oxidation stage.<sup>[49]</sup> Thus a dissimilar oxygen content in DC and MF films may be the reason. Despite a quite low oxygen partial pressure ( $p(\text{O}_2) \approx 10^{-13} \text{ Pa}$ ) over substrate during deposition, oxygen is chemically activated in plasma. Different discharge modes provide different excitation level and therefore different chemical activity of oxygen. We note here that according to the Raman spectroscopy data

(Figure S4b, Table S3) carbon is amorphous to larger extent in MF-films.

Platinum oxidation is also typical for Pt/C catalysts exposed to air,<sup>[50]</sup> although surface sensitive XPS analysis has not revealed any valuable difference between films in question. All measured Pt4f spectra can be fitted with the same model which includes three doublets with  $4f_{7/2}$  binding energies at  $\sim 72.3$  eV,  $\sim 73.6$  eV, and  $\sim 74.5$  eV (Figure 4). The 72.3 eV contribution is shifted from the energy characteristic for metallic Pt (71.2 eV)<sup>[51]</sup> by  $\sim 1.1$  eV. There are reports assigning shifts of up to  $+0.8$  eV to nano-crystallinity of metallic platinum.<sup>[52–54]</sup> The shift was shown to increase when particle size decreases and can even reach  $+1.3$  eV for  $\sim 1.5$  nm small Pt-particles.<sup>[55]</sup> Binding energy (BE) may also increase if metallic surface contains adsorbed oxygen / water molecules (Pt–O<sub>2 ads</sub>/Pt–OH<sub>2 ads</sub>) which cause positive charging of Pt-atoms.<sup>[53,54]</sup> Physically adsorbed water appears when our samples were exposed to air after deposition. From the O1s spectrum (Figure S3) we see that the contribution at 534.8 eV which represents adsorbed water<sup>[56]</sup> is significant. One may speculate that water gets bound to platinum atoms at the surface stronger (implying partial Pt<sup>+δ</sup>→<sup>−δ</sup>OH<sub>2</sub> charge transfer) due to their reduced coordination at this particle size. To sum up, higher BE of the Pt 4f-duplet in question is probably a result of two interrelated factors described.

The doublet at 73.6 eV binding energy is usually attributed to Pt<sup>+2</sup> (PtO/Pt(OH)<sub>2</sub>).<sup>[51–54,57]</sup> This contribution is for all films analysed about 3.5 times smaller than the one at 72.3 eV. The 74.5 eV contribution clearly corresponds to the Pt<sup>+4</sup> (PtO<sub>2</sub>/Pt(OH)<sub>2</sub>/Pt(OH)<sub>4</sub>) state.<sup>[56,58]</sup> Since the O1s emission at 530.6 eV

which is commonly assigned to O<sup>−2</sup> contribution has a noticeably smaller peak area compared to the feature at 532.3 eV that is usually assigned to OH<sup>−</sup><sup>[51,57]</sup> we admit a high hydrolysatation degree of oxides. This is consistent with a presence of considerable amount of adsorbed water.

Based on this judgement the analysed data are summarized for all samples in Table 1. Comparing deposition modes, we see that the DC-films are generally more oxidized in a form of Pt<sup>+2</sup> than the MF-films. This is apparently interrelated to the Pt<sup>+δ</sup> contribution which is inverse for the deposition modes being compared. We apparently deal here with the consequences of air exposure since no oxidation of platinum was detected in the bulk of the films (see above). At the same time the C1s spectra reveal almost no difference in oxidation degree of carbon for DC and MF films (Table S2).

Prior to the electrocatalytic measurements we took a closer look at the electrical properties of our films. To some extent, the in-plane resistivity gives an idea about the electrical barrier for electrolysis. A value of  $< 10 \Omega\cdot\text{m}$  should be targeted.<sup>[58]</sup> Since porous carbon support usually serves as a conductive carrier for Pt-nanoparticles in electrocatalysis,<sup>[59]</sup> we studied if our GFS-process can produce a porous conductive carbon scaffold. The films revealing in XRR lowest density (highest porosity) shown a resistivity of about  $10^5 \text{ Ohm}\cdot\text{m}$  that is obviously too high for the application in question. Since the XRD patterns of Pt/C films do not show any carbon-related phases we assume that carbon is poorly conductive in GFS-films because of its nano-crystallinity and high defectiveness (see also Raman data in SI).

As presented in Table S1, the Pt/C-films obtained in MF-sputtering mode are more conductive than the ones deposited in DC-plasma. Figure S5 plots resistivity ( $\rho$ ) of the Pt/C-films on glass as a function of film thickness. The scaffold-based films do not fulfil the resistivity criterium ( $\rho < 10 \Omega\cdot\text{m}$ ) having an order of magnitude higher resistivity than the scaffold-free ones. This difference can be explained as follows: higher roughness of the carbon support gives for the same deposition time smaller effective Pt/C thickness (see insets in Figure S5). Since we measure the in-plane conductivity the path of current over rough surface is longer, and its percolation can be poorer. Interestingly, the resistivity notably decreases with the thickness for the single Pt/C films. This effect points at an increasing interconnectivity between Pt-nanoparticles in thicker layers. It can be attributed to a heating by plasma during deposition. With deposition time this effect accumulates. The data given in Table S3 illustrate such an effect by somewhat higher crystallization extent of carbon in thicker film but only in case of using MF-plasma. Still, carbon is predominantly nanocrystalline and

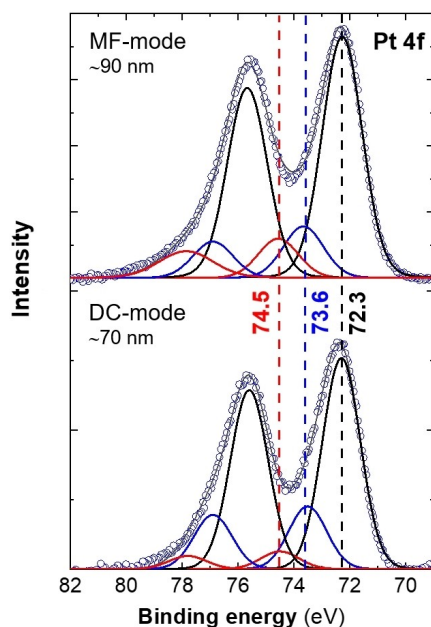


**Figure 4.** Pt4f spectra measured for the Pt/C films sputtered in different plasma modes (specified in each plot together with film thickness). Fitting with three contributions (mixed Gaussian-Lorentzian function) was applied under constrained FWHM conditions (open circle – experimental data, solid lines – fitted data). The dashed lines and given binding energies correspond to the Pt $4f_{7/2}$  maxima.

**Table 1.** Quantification (area distribution in %) of the components as fitted in Pt4f spectra for Pt/C-films of different thickness deposited in different modes.

Pt state	(Pt $4f_{5/2}$ + Pt $4f_{7/2}$ ) peaks area in [%]/sample			
	DC ~70 nm	DC ~240 nm	MF ~90 nm	MF ~240 nm
Pt <sup>+δ</sup>	72.52	73.41	74.57	76.66
Pt <sup>+2</sup>	21.76	20.71	18.38	17.79
Pt <sup>+4</sup>	5.72	5.88	7.05	5.55

defect-rich and acts more like an isolator than a conductor in our films. This factor has not allowed us to evaluate HER-performance of the scaffold-based films at this stage.

For the evaluation of the electrocatalytic performance, we have chosen the DC and MF films with an average thickness  $\sim 70$  and  $\sim 90$  nm, respectively (Table S1). The performance in the hydrogen evolution reaction (HER) was studied in a typical RDE setup in sulphuric acid (0.5 mol/l). Developed in the StrataGem software EPMA data have given the geometric Pt-loading of 55.7 and 84.5  $\mu\text{g}_{\text{Pt}}/\text{cm}^2$  for the DC and MF films respectively. The C-loading for the same films was found to be 10.9 and 16.1  $\mu\text{g}_{\text{C}}/\text{cm}^2$ . The catalyst films show a stable HER performance. In the first 50 cycles of cyclic voltammetry the catalysts demonstrated no significant changes (Figure 5a,b). Also, during a subsequent stability sequence at  $-50$  mA/cm<sup>2</sup> the catalysts reached stable current density at circa  $-10$  mV vs. RHE (Figure 5c,d). The DC film had a minor degradation over time whereas the MF-film showed an increase in activity after 10 h of testing reaching a lower overpotential of  $-7$  mV vs. RHE after 20 h of testing.

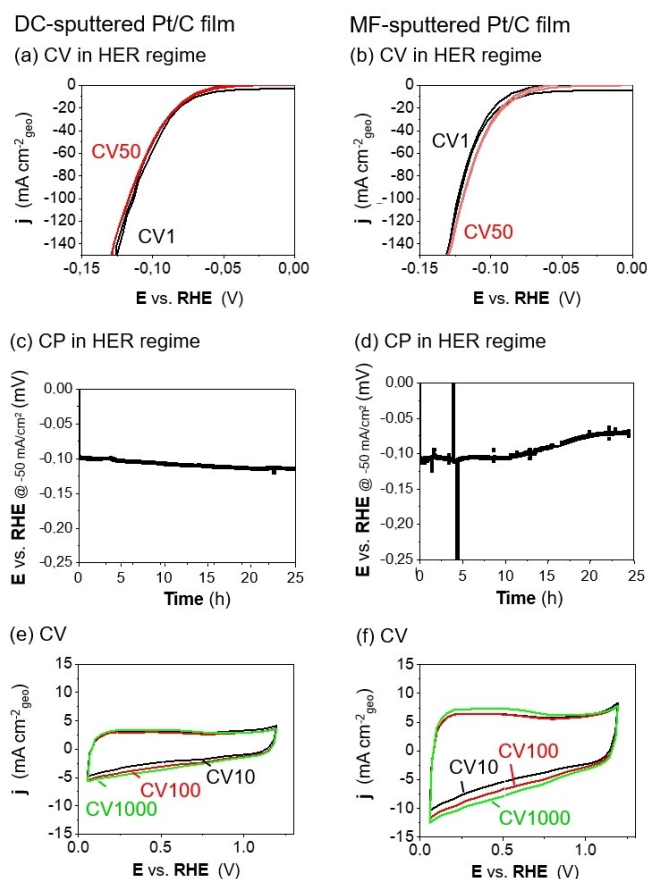


**Figure 5.** Cyclic voltammetric (CV) and chronopotentiometric (CP) testing in 0.5 M sulfuric acid of both kinds of Pt/C catalyst films deposited on a glassy carbon substrate. All potentials are iR-corrected. a,b) 1<sup>st</sup> and 50<sup>th</sup> cycle of CV measurement in the HER regime with 20 mV/s. c,d) CP measurement in the HER regime. The spikes are caused by gas formation at the surface of the working electrode. e,f) 1000<sup>th</sup> cycle of CV testing between 0.05 V and 1.20 V with 100 mV/s showing ulterior profiles of Pt in sulphuric acid.

In terms of Pt-mass activity, the catalysts reached a current density of 0.9 mA/ $\mu\text{g}_{\text{Pt}}$  for the DC- and 0.4 mA/ $\mu\text{g}_{\text{Pt}}$  for the MF-film at  $-10$  mV versus RHE. In both cases it is a significantly weaker performance than that of a typical Pt/C catalyst described in literature. Figures 5e and 5f show that the electrochemically accessible surface area of the Pt/C catalyst film does not considerably change over a sequence of 1000 cycles. An estimation of the active area of surface Pt (ECSA<sub>Pt</sub>) cannot be done since no characteristic H<sub>upd</sub>-features are observable. Obviously, the GFS Pt/C films contain a significant part of *nc*-Pt which is not accessible for the electrolyte or the gas exchange is restrained. To compare, a thin catalyst film made from an ink of small Pt nanoparticles on Vulcan carbon deposited together with Nafion (3  $\mu\text{g}_{\text{Pt}}/\text{cm}^2$ ) can reach a high current density of  $-100$  mA/cm<sup>2</sup> at an overpotential of  $-10$  mV versus RHE leading to a mass activity of  $\sim 33$  mA/ $\mu\text{g}_{\text{Pt}}$  when tested under similar conditions.<sup>[47]</sup> Nevertheless, thick catalyst films with high geometric catalyst loadings ( $> 5$  mg<sub>Pt</sub>/cm<sup>2</sup>) are still of interest for use in long-lasting cathodes in industrial electrolyser cells.<sup>[60]</sup>

A higher catalytic activity of the DC film as compared to the MF film can be caused by a different nanostructure: larger grains (in TEM) with more defects (smaller areas of coherent scattering in XRD) in former case. Another difference to point is a presumably lower bulk oxidation degree of platinum in the DC film.

## Conclusions

This work presented nanostructured Pt/C-composite electrocatalytic films deposited by a hollow cathode gas-flow sputtering method in a single step. No intentional heating or post-treatment was used. Two plasma generation regimes: direct current and unipolar middle frequency pulsed are compared. The films were characterised to determine structural and chemical states of platinum and carbon. Carbon in the GFS-films was found to be in rather non-graphitic and poorly conductive state. The composite Pt/C-films demonstrated stable and reproducible HER-performance. However, the Pt-load was yet too large and therefore the corresponding Pt-mass activity was yet too low. Extreme chemical activity of the Pt/C-surface right after deposition leads to platinum oxidation by oxygen when exposed to air. This factor may seriously downgrade catalytic activity. Water itself remains rather chemisorbed and therefore safe transfer into the electrochemical cell is critical.

Much higher sputtering rate of Pt in a wide power range in contrast to the same of carbon obstructs to recommend single step sputtering of Pt/C-films at this development stage. The two-step approach providing much lower Pt-load when a porous carbon scaffold is sputtered at first and a thin composite Pt/C-film is deposited on top should be further improved targeting better conductivity of carbon films. The GFS method possessing generally higher deposition rates than the magnetron sputtering and having no need for expensive high vacuum equipment was found to be applicable for deposition of carbon films. Their lower resistivity is proposed to achieve using higher

substrate temperature in combination with adding hydrogen containing reactive gas to prevent carbon oxidation.

To sum up, the presented single-step fabrication of Pt/C catalysts can be a promising alternative to establish a new synthesis routine for electrocatalysts.

## Supporting Information Summary

Supporting information includes further experimental data such as sheet resistance, elemental composition, XRR and electron diffraction patterns, as well as Raman and XPS (C1s, O1s) spectra. These data help to understand the difference between deposition modes and comprehend the issue of highly resistive carbon. The O1s spectra provide more insights to the chemical state of platinum on the surface. Additional references are cited within the Supporting Information.<sup>[61–67]</sup>

## Acknowledgements

Authors thank Benjamin Paul (Institute for Technical Chemistry, TU Berlin), Dr. Christian Günther (ZELMI, TU Berlin) and Sri Hari Bharath Vinoth Kumar (Chair Technology for Thin Film Devices, TU Berlin) for support in special preparation of the samples. Dr. Markus R. Wagner (Institute of Solid-State Physics, TU Berlin) provided the Raman spectroscopy infrastructure. We acknowledge the financial support of Bundesministerium für Bildung und Forschung (CatLab project, Förderkennzeichen 03EW0015A). Open Access funding enabled and organized by Projekt DEAL.

## Conflict of Interests

The authors declare no conflict of interest.

## Data Availability Statement

The data that support the findings of this study are available from the corresponding author upon reasonable request.

**Keywords:** electrocatalysis · gas flow sputtering · hydrogen evolution reaction · nanomaterials · Pt/C film

- [1] M. Carmo, D. L. Fritz, J. Mergel, D. Stolten, *Int. J. Hydrogen Energy* **2013**, *38*, 4901–4934.
- [2] E. W. McFarland, H. Metiu, *Chem. Rev.* **2013**, *113*, 4391–4427.
- [3] M. Chhetri, S. Sultan, C. N. R. Rao, *PNAS* **2017**, *114* (34), 8986–8990.
- [4] A. Xie, N. Xuan, K. Ba, Z. Sun, *ACS Appl. Mater. Interfaces* **2017**, *9*, 4643–4648.
- [5] S. J. Gutić, A. S. Dobrota, M. Leetmaa, N. V. Skorodumova, S. V. Mentus, I. A. Pašti, *Phys. Chem. Chem. Phys.* **2017**, *19*, 13281.
- [6] W. J. Lee, S. Bera, C. M. Kim, E.-K. Koh, W.-P. Hong, S.-J. Oh, E. A. Cho, S.-H. Kwon, *J. Mater. Chem. A* **2021**, *9*, 17223.
- [7] N. Hodnik, L. Romano, P. Jovanovic, F. Ruiz-Zepeda, M. Bele, F. Fabbri, L. Persano, A. Camposo, D. Pisignano, *ACS Appl. Nano Mater.* **2020**, *3*, 9880–9888.

- [8] A. H. Ghanim, J. G. Koonce, B. Hasa, A. M. Rassoolkhani, W. Cheng, D. W. Peate, J. Lee, S. Mubeen, *Front. Chem.* **2018**, *6*:523.
- [9] Y. Li, R. T. Yang, *J. Phys. Chem. C* **2007**, *111*, 11086–11094.
- [10] Z. Liu, X. Y. Ling, X. Su, J. Y. Lee, *J. Phys. Chem. B* **2004**, *108*, 8234–8240.
- [11] S. H. Joo, S. J. Choi, I. Oh, J. Kwak, Z. Liu, O. Terasaki, R. Ryoo, *Nature* **2001**, *412*, 169–172.
- [12] F. Hasché, M. Oezaslan, P. Strasser, *Phys. Chem. Chem. Phys.* **2010**, *12*, 15251–15258.
- [13] Y. Li, H. Wang, L. Xie, Y. Liang, G. Hong, H. Dai, *J. Am. Chem. Soc.* **2011**, *133*, 7296–7299.
- [14] V. Lordi, N. Yao, J. Wei, *Chem. Mater.* **2001**, *13*, 733–737.
- [15] X. Jining, W. Shouyan, L. Arayasomayajula, V. K. Varadan, *Nanotechnology* **2007**, *18*, 065503.
- [16] C. Tang, D. Wang, Z. Wu, B. Duan, *Int. J. Hydrogen Energy* **2015**, *40*, 3229–3237.
- [17] R. Garcia, M. Besson, P. Gallezot, *Appl. Catal. A* **1995**, *127*, 165–176.
- [18] H. Zhang, H. Cui, *Langmuir* **2009**, *25*, 2604–2612.
- [19] Y. Garsany, J. Ge, J. St-Pierre, R. Rocheleau, K. Swider-Lyons, *ECS Trans.* **2013**, *58*, 1233–1241.
- [20] Y. Garsany, J. Ge, J. St-Pierre, R. Rocheleau, K. E. Swider-Lyons, *J. Electrochem. Soc.* **2014**, *161*, F628–F640.
- [21] H.-C. Tu, W.-L. Wang, C.-C. Wan, Y.-Y. Wang, *J. Phys. Chem. B* **2006**, *110*, 15988–15993.
- [22] S. S. Kocha, J. W. Zack, S. M. Alia, K. C. Neylerlin, B. S. Pivovar, *ECS Trans.* **2013**, *50*, 1475–1485.
- [23] K. Shinozaki, B. S. Pivovar, S. S. Kocha, *ECS Trans.* **2013**, *58*, 15–26.
- [24] D. Feng, Y. Lv, Z. Wu, Y. Dou, L. Han, Z. Sun, Y. Xia, G. Zheng, D. Zhao, *J. Am. Chem. Soc.* **2011**, *133*, 15148–15156.
- [25] Z. Qiang, Y. Zhang, Y. Wang, S. M. Bhaway, K. A. Cavicchi, B. D. Vogt, *Carbon* **2015**, *82*, 51–59.
- [26] Z. Qiang, J. Xue, G. E. Stein, K. A. Cavicchi, B. D. Vogt, *Langmuir* **2013**, *29*, 8703–8712.
- [27] C. Liang, Z. Li, S. Dai, *Angew. Chem. Int. Ed.* **2008**, *47*, 3696–3717.
- [28] S. Tanaka, A. Doi, N. Nakatani, Y. Katayama, Y. Miyake, *Carbon* **2009**, *47*, 2688–2698.
- [29] S. Tanaka, N. Nishiyama, Y. Egashira, K. Ueyama, *Chem. Commun.* **2005**, *16*, 2125–2127.
- [30] L. Chuenchom, R. Kraehnert, B. M. Smarsly, *Soft Matter* **2012**, *8*, 10801–10812.
- [31] H. Teysez, F. Scheth in *Ordered Mesoporous Materials as Catalysts*, Vol. 55 (Eds.: C. G. Bruce, C. J. Friederike), Academic Press, San Diego, **2012**, p. 127.
- [32] J. Jin, N. Nishiyama, Y. Egashira, K. Ueyama, *Microporous Mesoporous Mater.* **2009**, *118*, 218–223.
- [33] M. Comotti, W.-C. Li, B. Spliethoff, F. Scheth, *J. Am. Chem. Soc.* **2006**, *128*, 917–924.
- [34] O. K. Alexeeva, V. N. Fateev, *Int. J. Hydrogen Energy* **2016**, *41*, 3373–3386.
- [35] I. Y. Cha, M. Ahn, S. J. Yood, Y.-E. Sung, *RSC Adv.* **2014**, *4*, 38575.
- [36] P. Brault, A. Caillard, S. Baranton, M. Mougnot, S. Cuyner, C. Coutanceau, *ChemSusChem* **2013**, *6*, 1168–1171.
- [37] A. Ostroverkh, V. Johánek, M. Dubau, P. Kůs, I. Khalakhan, B. Šmíd, R. Fiala, M. Václavů, Y. Ostroverkh, V. Matolín, *J. Hydrogen Energy* **2019**, *44*, 19344–19356.
- [38] K. Fu, L. Zeng, J. Liu, M. Liu, S. Li, W. Guo, Y. Gao, M. Pan, *J. Alloys Compd.* **2019**, *815*, 152374.
- [39] W. Jeong, I. Chang, S. Ryu, C. Zheng, S. Won Cha, T. Park, *AIP Adv.* **2019**, *9*, 095016.
- [40] E. Medvedeva, A. Baranov, N. Samotaev, *Iop. Conf. Ser. Mater. Sci. Eng.* **2019**, *498*, 012027.
- [41] M. Umeda, K. Nagai, M. Shibamine, M. Inoue, *Phys. Chem. Chem. Phys.* **2010**, *12*, 7041–7049.
- [42] A. Ostroverkh, M. Dubau, V. Johánek, M. Václavů, B. Šmíd, K. Veltruská, Y. Ostroverkh, R. Fiala, V. Matolín, *Fuel Cells* **2018**, *18*, 51–56.
- [43] G. Schäfer, K. H. Schönbach, In: *Physics and Applications of Pseudosparks*, Vol. 219 (Eds. M. A. Gundersen and G. Schaefer) NATO ASI Series B: Physics, Plenum, New York, **1990** pp. 55–76.
- [44] T. Kälber, T. Jung, *Surf. Coat. Technol.* **1998**, *98*, 1116–1120.
- [45] K. Ishii, *J. Vac. Sci. Technol.* **1989**, *A7*, 256–258.
- [46] M. Birkholz, U. Albers, T. Jung, *Surf. Coat. Technol.* **2004**, *179*, 276–285.
- [47] D. Bernsmeier, R. Sachse, M. Bernicke, R. Schmack, F. Kettmann, J. Polte, R. Kraehnert, *J. Catal.* **2019**, *369*, 181–189.
- [48] K. Wasa, I. Kanno, H. Kotera (Eds.), *Handbook of Sputter Deposition Technology* (Second Edition), William Andrew Publishing **2012**, p. 41.
- [49] M. A. van Spronsen, J. W. M. Frenken, I. M. N. Groot, *Nat. Commun.* **2017**, *8*, 429.

- [50] R. Banerjee, D. A. Chen, S. Karakalos, M.-L. C. Piedboeuf, N. Job, J. R. Regalbutto, *ACS Appl. Nano Mater.* **2018**, *1*, 5876–5884.
- [51] J. Chastain (Ed.), *Handbook of X-ray photoelectron spectroscopy*, Perkin-Elmer Corp. USA, **1992**, 261 p. ISBN 0-9627026-2-5.
- [52] S. Strbac, S. Petrovic, R. Vasilic, J. Kovac, A. Zalar, Z. Rakocevic, *Electrochim. Acta* **2007**, *53*, 998–1005.
- [53] D. Riassetto, C. Holtzinger, M. Messaoud, S. Briche, G. Berthomé, F. Roussel, L. Rapenne, M. Langlet, *J. Photochem. Photobiol. A* **2009**, *202*, 214–220.
- [54] G. Wang, J. Parrondo, Ch. He, Y. Li, V. Ramani, *J. Elec.-chem. Soc.* **2017**, *164*, F1307-F1315.
- [55] R. J. Isaifan, S. Ntais, E. A. Baranova, *Appl. Catal. A* **2013**, *15*, 87–94.
- [56] X. Kong, D. Castarede, A. Boucly, L. Artiglia, M. Ammann, Th. Bartels-Rausch, E. S. Thomson, Jan B. C. Pettersson, *J. Phys. Chem. C* **2020**, *124*, 5263–5269.
- [57] M. Peukert, *Electrochim. Acta* **1984**, *29*, 1315–1320.
- [58] W. Suh, P. Ganesan, B. Son, H. Kim, S. Shanmugam, *Int. J. Hydrogen Energy* **2016**, *41*, 12983–12994.
- [59] M. Bernicke, D. Bernsmeier, B. Paul, R. Schmack, A. Bergmann, P. Strasser, E. Ortel, R. Kraehnert, *J. Catal.* **2019**, *376*, 209–218.
- [60] K. Novikova, A. Kuriganova, I. Leontyev, E. Gerasimova, O. Maslova, A. Rakhmatullin, N. Smirnova, Y. Dobrovolsky, *Electrocatalysis* **2018**, *9*, 22–30.
- [61] G. Beamson, D. Briggs, *The Scienta ESCA300 Database Wiley Interscience*, **1992**.
- [62] M. Carmo, D. L. Fritz, J. Mergel, D. Stolten, *Int. J. Hydrogen Energy* **2013**, *38*, 4901–4934.
- [63] A. Ganguly, S. Sharma, P. Papakonstantinou, J. Hamilton, *J. Phys. Chem. C* **2011**, *115*, 17009–17019.
- [64] T. H. T. Vu, T. T. T. Tran, H. N. T. Le, L. T. Tran, P. H. T. Nguyen, H. T. Nguyen, N. Q. Bui, *Electrochim. Acta* **2015**, *161*, 335–342.
- [65] J. B. Wu, M. L. Lin, X. Cong, H. N. Liu, P. H. Tan, *Chem. Soc. Rev.* **2018**, *47*, 1822–1873.
- [66] A. C. Ferrari, J. Robertson, *Phys. Rev. B* **2000**, *61*, 14095.
- [67] M. S. Dresselhaus, A. Jorio, M. Hofmann, G. Dresselhaus, R. Saito, *Nano Lett.* **2010**, *10*, 751–758.

---

Manuscript received: October 30, 2022  
Revised manuscript received: May 5, 2023  
Accepted manuscript online: May 9, 2023  
Version of record online: June 1, 2023